Electronic Supplementary Material (ESI) for Journal of Materials Chemistry A.

—Supplementary Information—

A Chemical Map of NaSiCON Electrode Materials for Sodium-ion Batteries

Baltej Singh,[1#] Ziliang Wang,[1#] Sunkyu Park,[2,3,4] Gopalakrishnan Sai Gautam,[5] Jean-Noël Chotard,[2,4,7] Laurence Croguennec,[3,4,6] Dany Carlier,[3,4,6] Anthony K. Cheetham,[1,7] Christian Masquelier,[2,4,6,^] and Pieremanuele Canepa[1,8] *

[1]Department of Materials Science and Engineering, National University of Singapore, Singapore 117575, Singapore

[2]Laboratoire de Réactivité et de Chimie des Solides (LRCS), CNRS UMR 7314, Université de Picardie Jules Verne, 80039 Amiens Cedex, France

[3]CNRS, Univ. Bordeaux, Bordeaux INP, ICMCB, UMR CNRS 5026, F-33600, Pessac, France

[4]RS2E, Réseau Français sur le Stockage Electrochimique de l'Energie, FR CNRS 3459, F-80039 Amiens Cedex 1, France.

[5]Department of Materials Engineering, Indian Institute of Science, Bengaluru, 560012, Karnataka, India

[6]ALISTORE-ERI European Research Institute, FR CNRS 3104, Amiens, F-80039 Cedex 1, France.

[7]Materials Department and Materials Research Laboratory, University of California, Santa Barbara, California 93106, United States

[8]Chemical and Biomolecular Engineering, National University of Singapore, 4 Engineering Drive 4, Singapore, 117585

^christian.masquelier@u-picardie.fr and *pcanepa@nus.edu.sg

[#]these authors contributed equally

Table of Contents

S1 Convex Hull and Voltage Curves of $Na_xM_2(PO_4)_3$ Systems

Figures S1, **S2**, **S3, S4, S5, S6** and **S7** show the computed formation energies from DFT at 0 K and respective convex hulls (green solid lines and dots) for Na vacancy orderings as well as the corresponding intercalation voltage vs. Na/Na^+ as a function of Na concentration (x) in $Na_xM_2(PO_4)_3$, NaSICON, where M= Ti, V, Cr, Mn, Fe, Co and Ni. Red crosses represent Na vacancies orderings lying above the convex hull. Na vacancy orderings at specific compositions lying above the convex hull will always phase separate into the nearest stable configurations (lying on the convex hull).

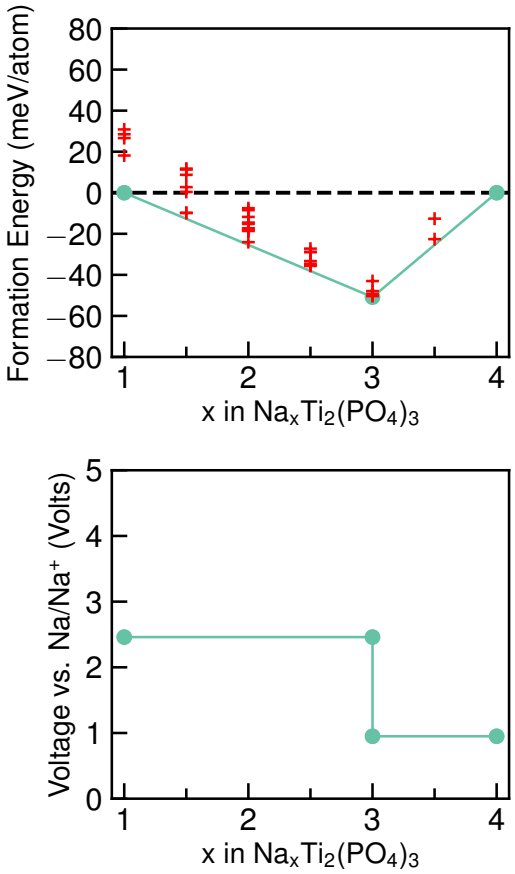

Figure S1 (upper panel) The computed formation energies and respective convex hulls (green line) for Na vacancy orderings as a function of Na concentration (x) in $Na_xTi_2(PO_4)_3$. (lower panel) The corresponding intercalation voltage vs. Na/Na^+ at different Na content. Note that x varies in the range $1 \leqslant x \leqslant 4$. The stable orderings forming the convex hull are displayed as green dots while the unstable orderings are given as red symbols.

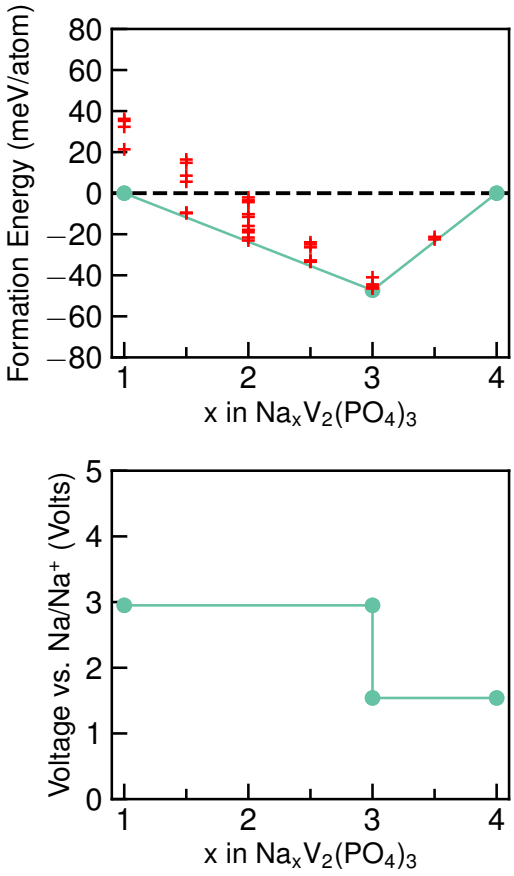

Figure S2 (upper panel) The computed formation energies and respective convex hulls (green line) for Na vacancy orderings as a function of Na concentration (x) in $Na_xV_2(PO_4)_3$. (lower panel) The corresponding intercalation voltage vs. Na/Na^+ at different Na content. Note that x varies in the range $1 \leq x \leq 4$. The stable orderings forming the convex hull are displayed as green dots while the unstable orderings are given as red symbols.

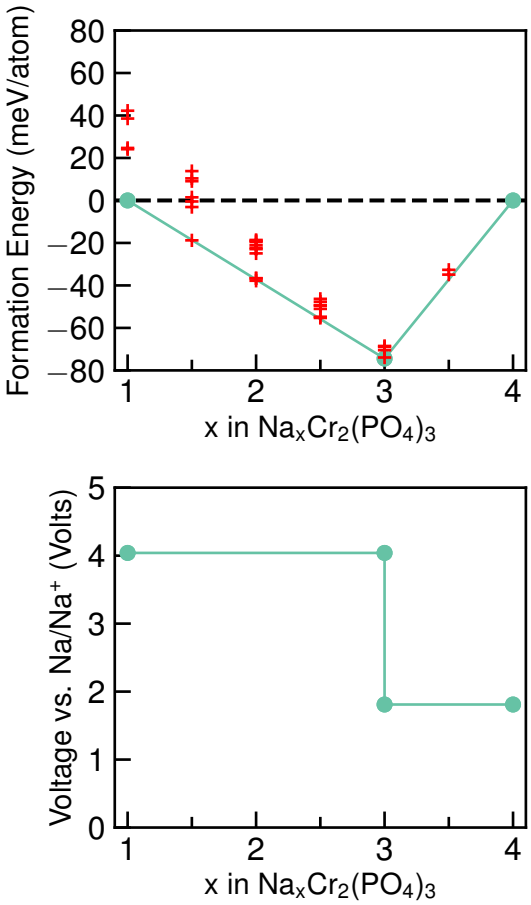

Figure S3 (upper panel) The computed formation energies and respective convex hulls (green line) for Na vacancy orderings as a function of Na concentration (x) in $Na_xCr_2(PO_4)_3$. (lower panel) The corresponding intercalation voltage vs. Na/Na^+ at different Na content. Note that x varies in the range $1 \leqslant x \leqslant 4$. The stable orderings forming the convex hull are displayed as green dots while the unstable orderings are given as red symbols.

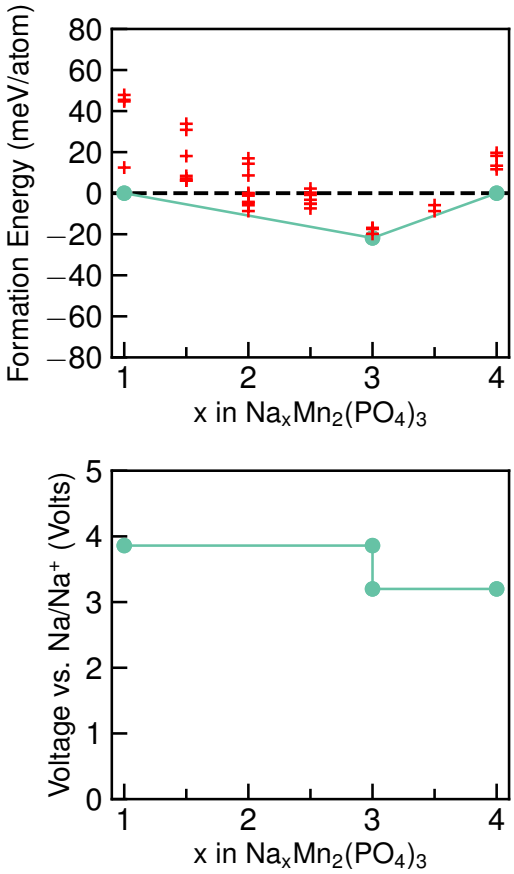

Figure S4 (upper panel) The computed formation energies and respective convex hulls (green line) for Na vacancy orderings as a function of Na concentration (x) in $Na_xMn_2(PO_4)_3$. (lower panel) The corresponding intercalation voltage vs. Na/Na^+ at different Na content. Note that x varies in the range $1 \leqslant x \leqslant 4$. The stable orderings forming the convex hull are displayed as green dots while the unstable orderings are given as red symbols.

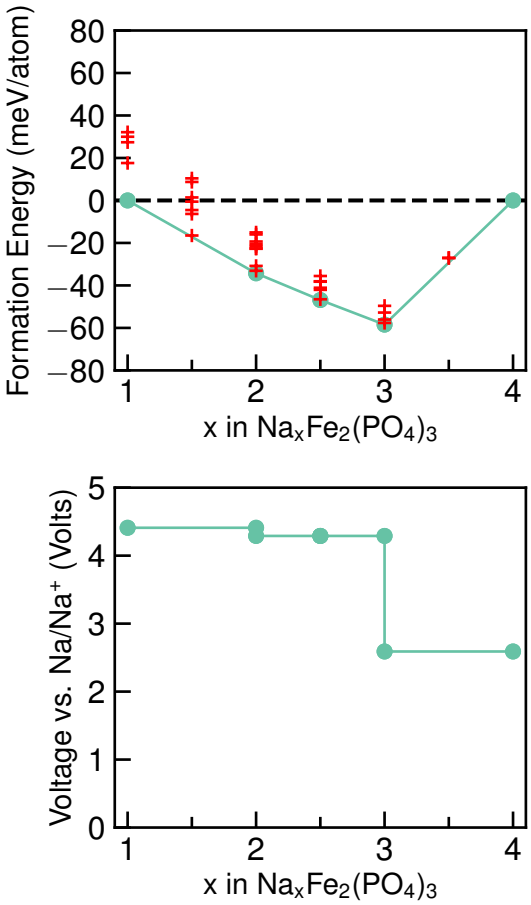

Figure S5 (upper panel) The computed formation energies and respective convex hulls (green line) for Na vacancy orderings as a function of Na concentration (x) in $Na_xFe_2(PO_4)_3$. (lower panel) The corresponding intercalation voltage vs. Na/Na^+ at different Na content. Note that x varies in the range $1 \leqslant x \leqslant 4$. The stable orderings forming the convex hull are displayed as green dots while the unstable orderings are given as red symbols.

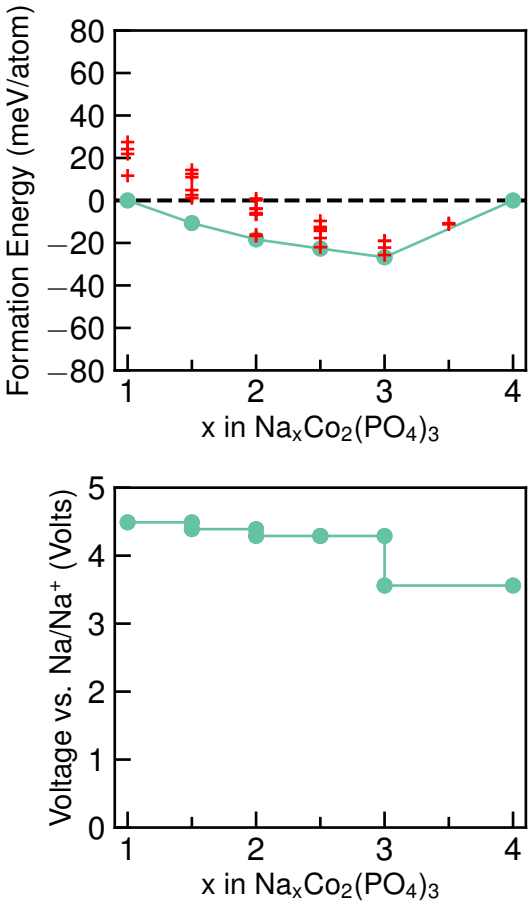

Figure S6 (upper panel) The computed formation energies and respective convex hulls (green line) for Na vacancy orderings as a function of Na concentration (x) in $Na_xCo_2(PO_4)_3$. (lower panel) The corresponding intercalation voltage vs. Na/Na^+ at different Na content. Note that x varies in the range $1 \leqslant x \leqslant 4$. The stable orderings forming the convex hull are displayed as green dots while the unstable orderings are given as red symbols.

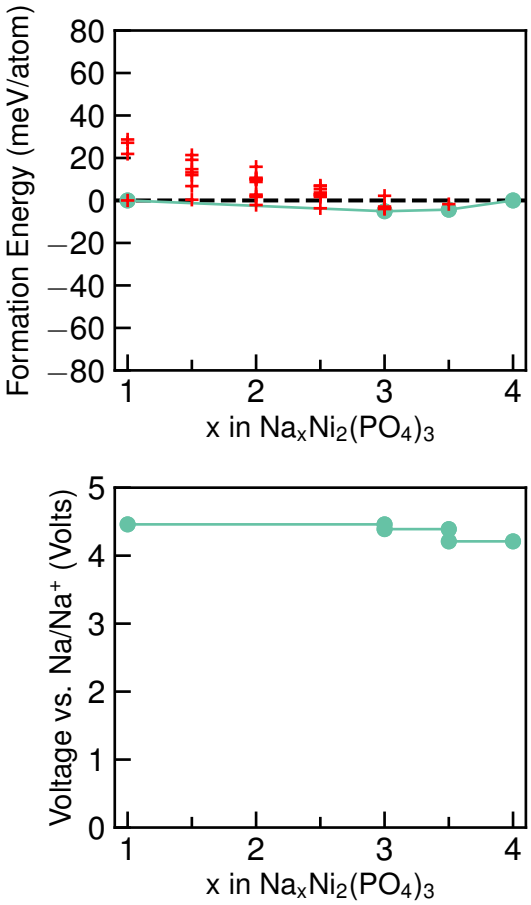

Figure S7 (upper panel) The computed formation energies and respective convex hulls (green line) for Na vacancy orderings as a function of Na concentration (x) in $Na_xNi_2(PO_4)_3$. (lower panel) The corresponding intercalation voltage vs. Na/Na^+ at different Na content. Note that x varies in the range $1 \leqslant x \leqslant 4$. The stable orderings forming the convex hull are displayed as green dots while the unstable orderings are given as red symbols.

S2 Comparison of Exchange and Correllation Functionals

Figures S8 shows the convex hull and the voltage curves of $Na_xV_2(PO_4)_3$ as the exchange and correlation functional is varied between GGA(PBE)+*U* [1,2] and the hybrid range-separated functional proposed by Heyd, Scuseria and Ernzerhof HSE06[3].

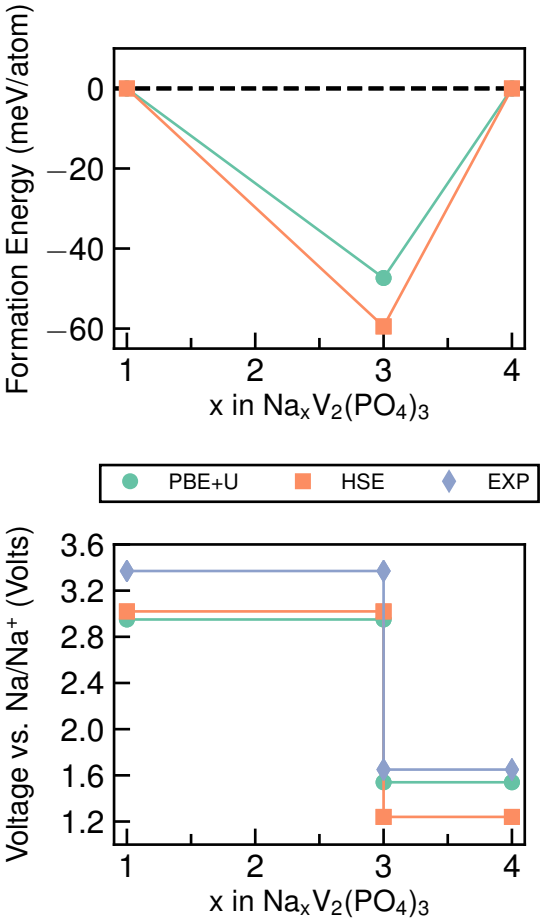

Figure S8 (upper panel) The computed formation energies and respective convex hulls with PBE+*U* (green line) and hybrid functional HSE06 (orange line) for Na vacancy orderings as a function of Na concentration ($1 \leqslant x \leqslant 4$) in $Na_xV_2(PO_4)_3$. (lower panel) The corresponding intercalation voltage vs. Na/Na^+ at different Na content are compared to experimental values (violet lines).[4]

From **Figure S8**, it can be observed that both GGA+*U* and HSE06 tend to underestimate the experimental voltages.

S3 Electronic Configuration of Transition Metals in NaSICON

The primitive unit cell of $Na_xM_2(PO_4)_3$ includes 2 f.u, and hence four transition metals (TM) per unit (simulation) cell. To assign the oxidation states of the transition metals, we analyzed the computed on-site magnetic moments (Bohr magneton μ_M), as indicated in **Tables S1** and **S2**.

Table S1 The computed magnetic moments (in μB) from DFT and assigned oxidation states for 3*d* transition metals in the octahedral coordination of NaSICON.

TM	Oxidation states and Magnetic moment			
Ti	II, μ = 1.9	III, μ = 1.0	IV, μ = 0.0	—
V	II, μ = 2.7	III, μ = 1.9	IV, μ = 1.0	V, μ = 0.0
Cr	II, μ = 3.8	III, μ = 3.0 – 2.9	IV, μ = 2.6 – 2.3	—
Mn	II, μ = 4.7 – 4.6	III, μ = 4.0 – 3.9	IV, μ = 3.4 – 3.3	—
Fe	II, μ = 3.8	III, μ = 4.3	—	—
Co	II, μ = 2.8	III, μ = 3.2 – 3.1	—	—
Ni	II, μ = 1.8	—	—	—

Our data demonstrates that the removal of the first Na from the formula $Na_4M^{III}M^{II}(PO_4)_3$ occurs via an oxidation of M^{2+} to M^{3+} to give $Na_3M^{III}M^{III}(PO_4)_3$. Further Na extraction give rise to $Na_2M^{III}M^{IV}(PO_4)_3$ and then to $Na_1M^{4+}M^{4+}(PO_4)_3$. Each of these Na extraction (like $Na_4M^{III}M^{II}(PO_4)_3$ to $Na_3M^{III}M^{III}(PO_4)_3$ etc.) actually involves the oxidation of two TM atoms (among four) per simulation cell. The intermediate minima at x= 3.5, 2.5 and 1.5 correspond to the reduction of only one transition metal (among four) sites M. For example, when Na is extracted from $Na_4V^{III}V^{II}(PO_4)_3$ (μ_M = ~1.9 on V^{3+} and 2.7 on V^{2+}), we obtain magnetic moments of 1.9 on all V^{3+} in $Na_3V_2(PO_4)_3$. Upon further deintercalation to $Na_2V_2(PO_4)_3$, the magnetic moments change to ~1.9 on V^{3+} and 1.0 on V^{4+}, respectively. However, assigning the exact oxidation state from magnetic moments become difficult especially for Ni, Co and Fe as they behave as metallic and electronic density is thus delocalized. For this purpose, their coordination environments are analyzed, as given in **Table S2.**

Table S2 The calculated site magnetic moment (first value) and corresponding average M-O octahedral bond length (second value) for various Na concentrations lying on the convex hull for Ni, Co, Fe and Mn based NaSICON.

NaSICON	Na Conc. (x)	Transition Metal Sites			
		M1	M2	M3	M4
$Na_xNi_2(PO_4)_3$	1	1.88, 2.03	1.88, 2.03	1.88, 2.03	1.88, 2.03
	3	1.74, 2.05	1.76, 2.05	1.74, 2.05	1.76, 2.05
	3.5	1.78, 2.05	1.75, 2.06	1.78, 2.05	1.75, 2.06
	4	1.78, 2.06	1.78, 2.06	1.78, 2.06	1.78, 2.06
$Na_xCo_2(PO_4)_3$	1	3.20, 1.97	3.16, 1.99	3.20, 1.97	3.16, 1.99
	1.5	3.17, 1.99	3.16, 2.00	3.16, 2.00	3.17, 1.99
	2	3.16, 2.01	3.16, 2.01	3.16, 2.01	3.16, 2.01
	2.5	3.16, 2.01	3.15, 2.02	3.15, 2.02	3.16, 2.01
	3	3.15, 2.02	3.15, 2.02	3.15, 2.02	3.15, 2.02
	4	3.12, 2.02	2.78, 2.11	3.12, 2.02	2.79, 2.12
$Na_xFe_2(PO_4)_3$	1	4.26, 1.99	4.26, 1.99	4.26, 1.99	4.26, 1.99
	2	4.33, 2.02	4.33, 2.02	4.33, 2.02	4.33, 2.02
	2.5	4.33, 2.03	4.33, 2.03	4.32, 2.03	4.33, 2.02
	3	4.33, 2.03	4.33, 2.03	4.33, 2.03	4.33, 2.03
	4	3.78, 2.15	4.31, 2.03	3.78, 2.15	4.31, 2.03
$Na_xMn_2(PO_4)_3$	1	3.31, 1.94	3.31, 1.94	3.16, 1.92	3.16, 1.92
	3	3.93, 2.06	3.93, 2.07	3.93, 2.07	3.93, 2.06
	4	4.59, 2.17	4.59, 2.17	4.07, 2.09	4.07, 2.08

S4 Density of States of Selected NaSICON Structures

The desity of states (DOSs) of selected mono-transition metal (TM) $Na_xM_2(PO_4)_3$ configurations, where M= Mn, Fe, Co and Ni are plotted in **Figure S9**, **S10, S11** and **S12** to investigate the electronic band gap. The elecronic density of states are calculated for the computed ground state configurations of $Na_xM_2(PO_4)_3$ at appropriate Na concentrations (x = 1, 3, 4). A dense Γ-centred Monkhorst-Pack *k*-point mesh with 75 divisions along each reciprocal lattice vector was applied to all the configurations, and the total energy was converged to within 10^{-5} eV/cell. The partial occupancies for each orbital are obtained with a smearing (of 0.05 eV width) scheme based on the tetrahedron method with Blöchl corrections. The calculated total and atom projected DOS are displayed for spin up and spin down states in the range of interest (–2.5 — 2 eV) around the Fermi energy. Unless for NaSICON configurations behaving as metals, the top of the Fermi energy is set at the top of the valance band. For all these NaSICON systems, the valence band near the fermi energy are dominantly occupied by 3d electron of TM, while the 2p O states lay at lower energies. Moreover, the TM states tend to dominate the conduction band.

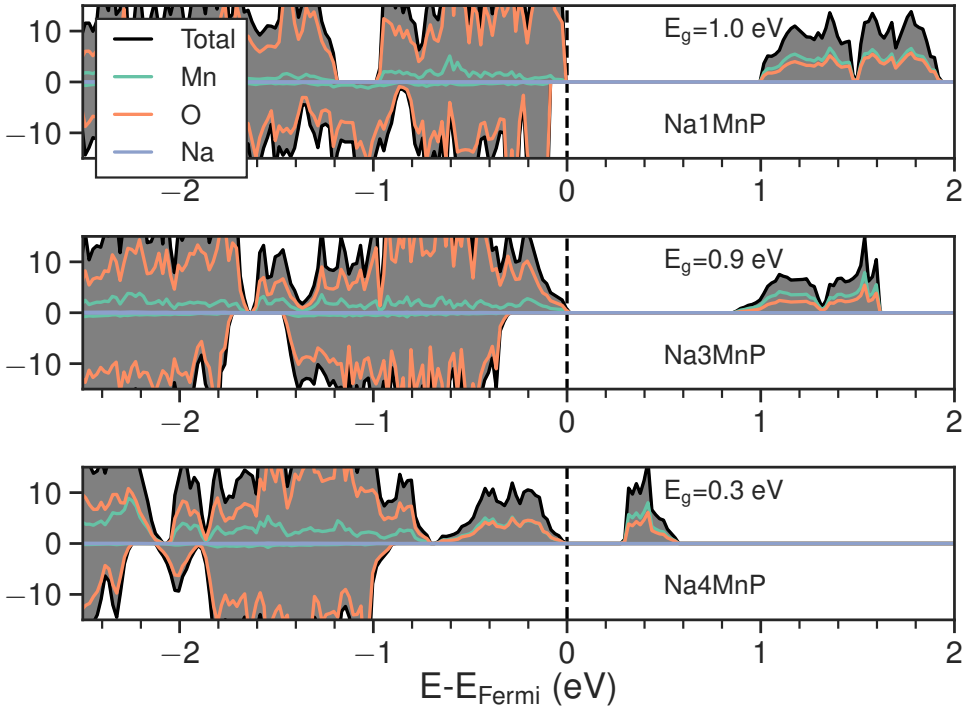

Figure S9 The total (gray) and atom projected (Mn aqua, O orange and Na blue) DOSs of $Na_xMn_2(PO_4)_3$ NaSICON, where Na concentration, x = 1, 3 and 4. The vertical line denotes the Fermi energy level and E_g is the calculated Band gap.

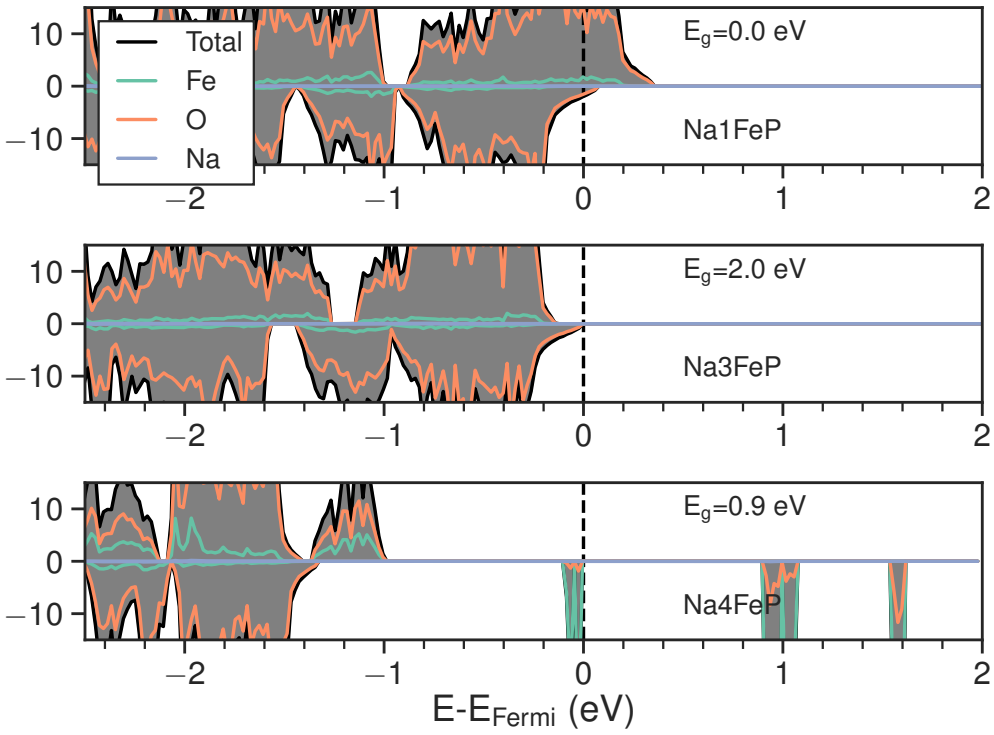

Figure S10 The total (gray) and atom projected (Fe aqua, O orange and Na blue) DOSs of $Na_xFe_2(PO_4)_3$ NaSICON, where Na concentration, x = 1, 3 and 4. The vertical line denotes the Fermi energy level and E_g is the calculated Band gap.

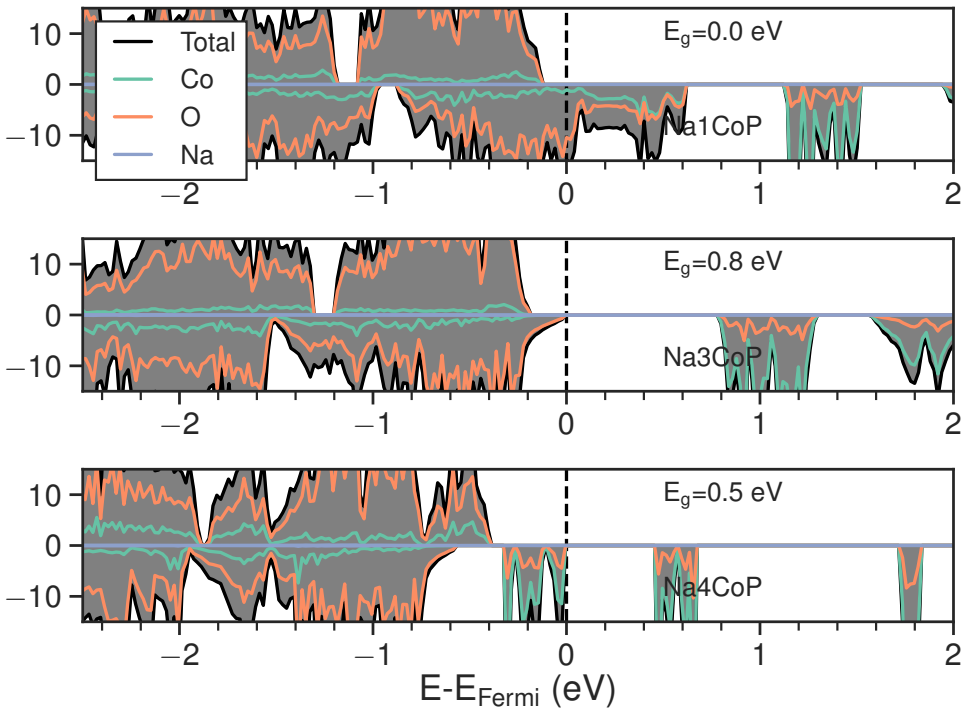

Figure S11 The total (gray) and atom projected (Co aqua, O orange and Na blue) DOSs of $Na_xCo_2(PO_4)_3$ NaSICON, where Na concentration, x = 1, 3 and 4. The vertical line denotes the Fermi energy level and E_g is the calculated Band gap.

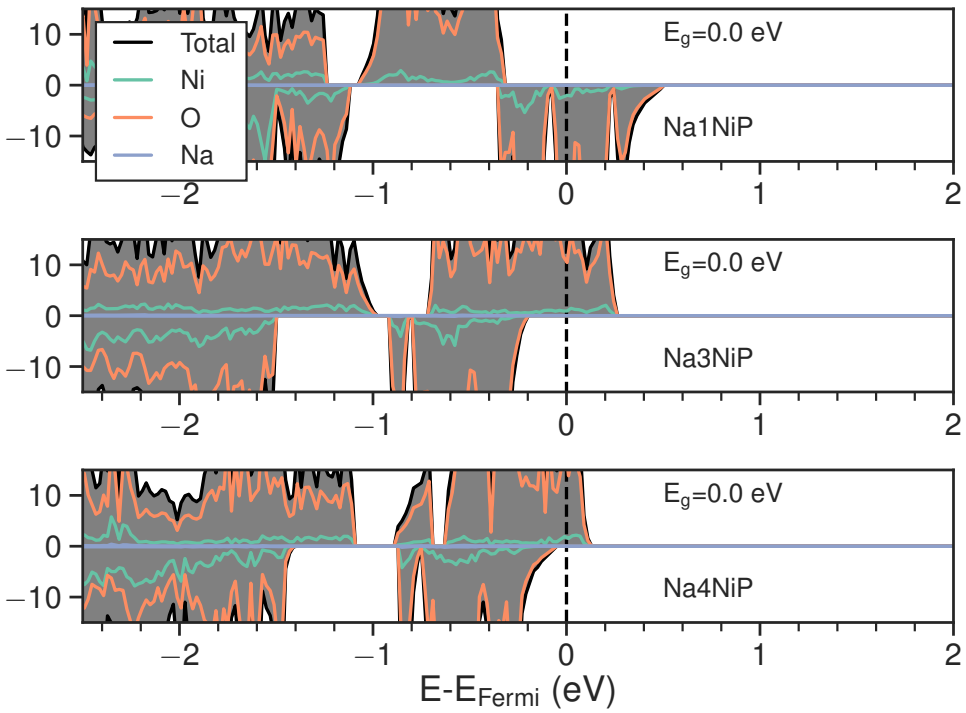

Figure S12 The total (gray) and atom projected (Ni aqua, O orange and Na blue) DOSs of $Na_xNi_2(PO_4)_3$ NaSICON, where Na concentration, x = 1, 3 and 4. The vertical line denotes the Fermi energy level and E_g is the calculated band gap.

S5 Convex Hull and Voltage Curves of Mixed $Na_xMM'(PO_4)_3$ Systems

Figures S13, **S14**, **S15**, **S16**, **S17**, **S18**, **S19**, **S20**, **S21**, **S22**, **S23**, **S24**, **S25**, **S26**, **S27**, **S28**, **S29**, **S30**, **S31**, **S32** and **S33** show the computed formation energies from DFT at 0 K and respective convex hulls (green solid lines and dots) for Na vacancy orderings, as well as the corresponding intercalation voltage vs. Na/Na^+ as a function of Na concentration (x) in mixed $Na_xMM'(PO_4)_3$ NaSICON, where M, M' = Ti, V, Cr, Mn, Fe, Co and Ni. Red crosses represent Na vacancies orderings lying above the convex hull.

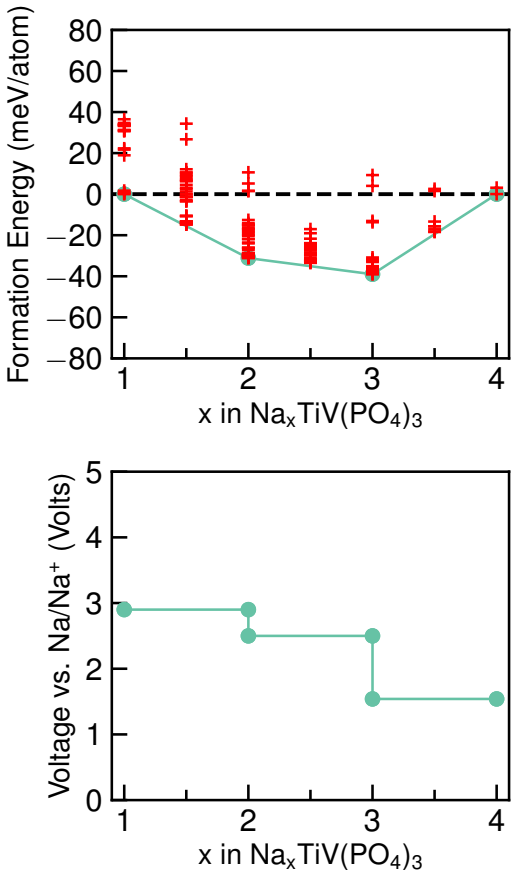

Figure S13 (upper panel) The computed formation energies and respective convex hulls (green line) for Na vacancy orderings as a function of Na concentration (x) in $Na_xTiV(PO_4)_3$. (lower panel) The corresponding intercalation voltage vs. Na/Na^+ at different Na content. Note that x varies in the range $1 \leq x \leq 4$. The stable orderings forming the convex hull are displayed as green dots while the unstable orderings are given as red symbols.

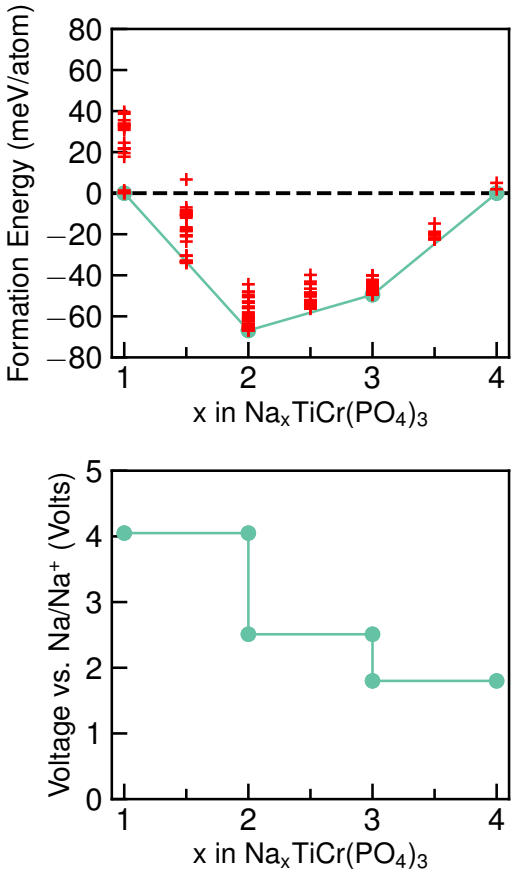

Figure S14 (upper panel) The computed formation energies and respective convex hulls (green line) for Na vacancy orderings as a function of Na concentration (x) in $Na_xTiCr(PO_4)_3$. (lower panel) The corresponding intercalation voltage vs. Na/Na^+ at different Na content. Note that x varies in the range $1 \leqslant x \leqslant 4$. The stable orderings forming the convex hull are displayed as green dots while the unstable orderings are given as red symbols.

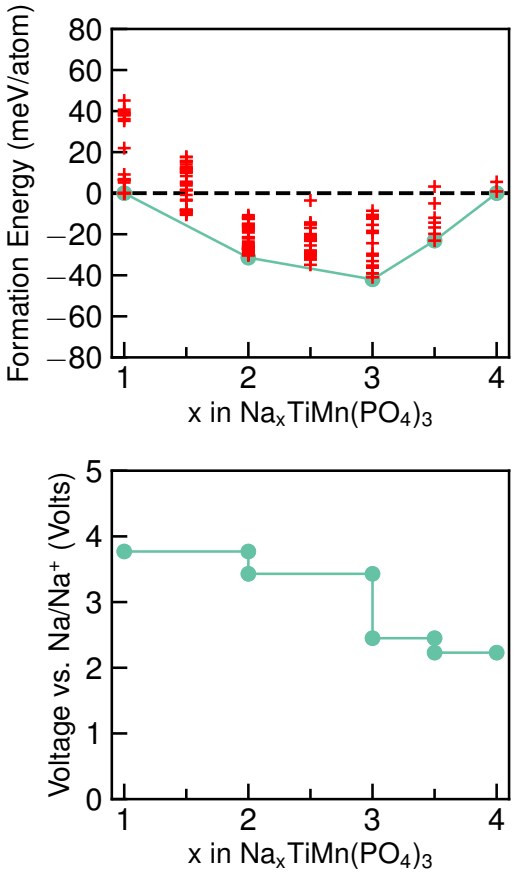

Figure S15 (upper panel) The computed formation energies and respective convex hulls (green line) for Na vacancy orderings as a function of Na concentration (x) in $Na_xTiMn(PO_4)_3$. (lower panel) The corresponding intercalation voltage vs. Na/Na^+ at different Na content. Note that x varies in the range $1 \leqslant x \leqslant 4$. The stable orderings forming the convex hull are displayed as green dots while the unstable orderings are given as red symbols.

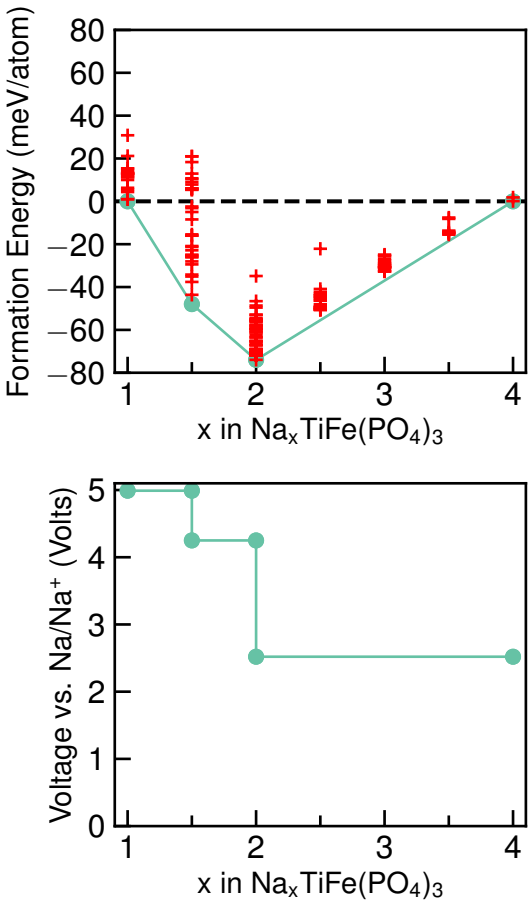

Figure S16 (upper panel) The computed formation energies and respective convex hulls (green line) for Na vacancy orderings as a function of Na concentration (x) in $Na_xTiFe(PO_4)_3$. (lower panel) The corresponding intercalation voltage vs. Na/Na^+ at different Na content. Note that x varies in the range $1 \leqslant x \leqslant 4$. The stable orderings forming the convex hull are displayed as green dots while the unstable orderings are given as red symbols.

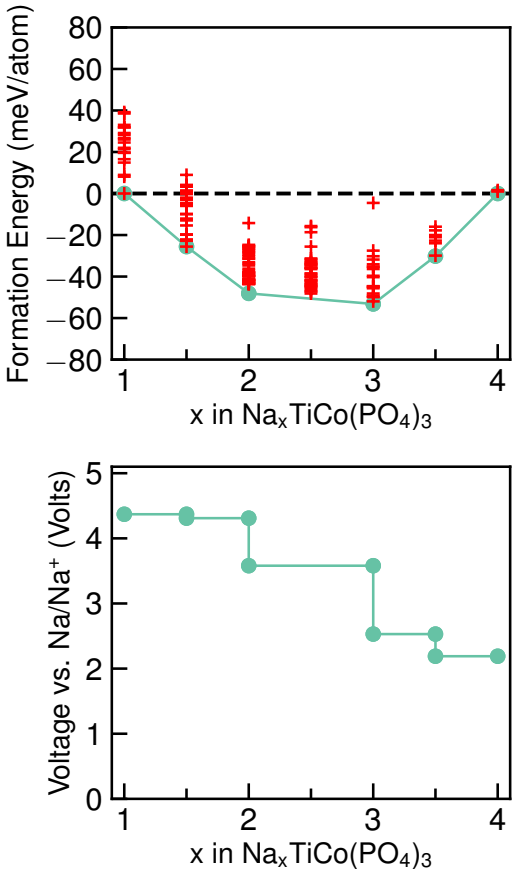

Figure S17 (upper panel) The computed formation energies and respective convex hulls (green line) for Na vacancy orderings as a function of Na concentration (x) in $Na_xTiCo(PO_4)_3$. (lower panel) The corresponding intercalation voltage vs. Na/Na^+ at different Na content. Note that x varies in the range $1 \leqslant x \leqslant 4$. The stable orderings forming the convex hull are displayed as green dots while the unstable orderings are given as red symbols.

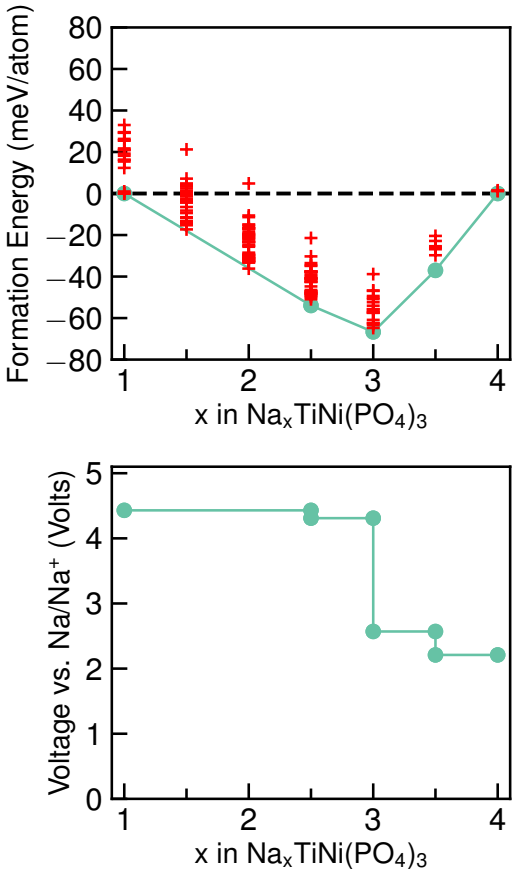

Figure S18 (upper panel) The computed formation energies and respective convex hulls (green line) for Na vacancy orderings as a function of Na concentration (x) in $Na_xTiNi(PO_4)_3$. (lower panel) The corresponding intercalation voltage vs. Na/Na^+ at different Na content. Note that x varies in the range $1 \leqslant x \leqslant 4$. The stable orderings forming the convex hull are displayed as green dots while the unstable orderings are given as red symbols.

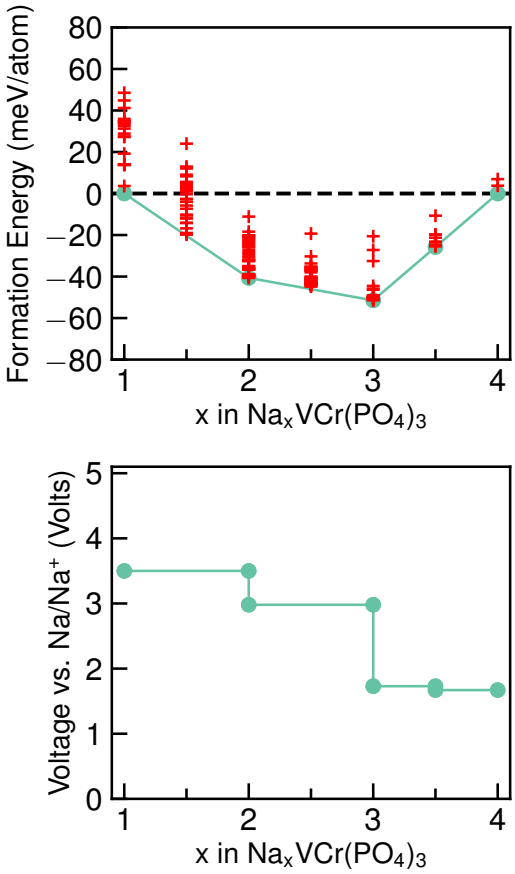

Figure S19 (upper panel) The computed formation energies and respective convex hulls (green line) for Na vacancy orderings as a function of Na concentration (x) in $Na_xVCr(PO_4)_3$. (lower panel) The corresponding intercalation voltage vs. Na/Na^+ at different Na content. Note that x varies in the range $1 \leqslant x \leqslant 4$. The stable orderings forming the convex hull are displayed as green dots while the unstable orderings are given as red symbols.

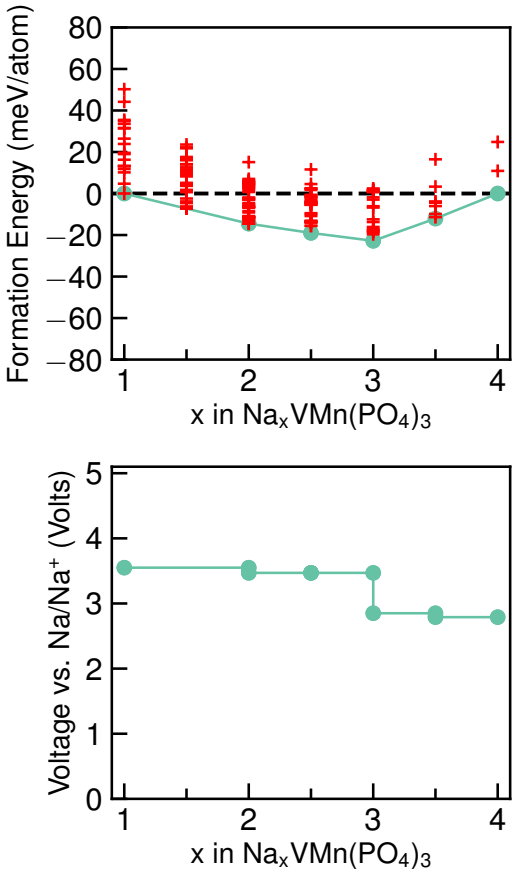

Figure S20 (upper panel) The computed formation energies and respective convex hulls (green line) for Na vacancy orderings as a function of Na concentration (x) in $Na_xVMn(PO_4)_3$. (lower panel) The corresponding intercalation voltage vs. Na/Na^+ at different Na content. Note that x varies in the range $1 \leqslant x \leqslant 4$. The stable orderings forming the convex hull are displayed as green dots while the unstable orderings are given as red symbols.

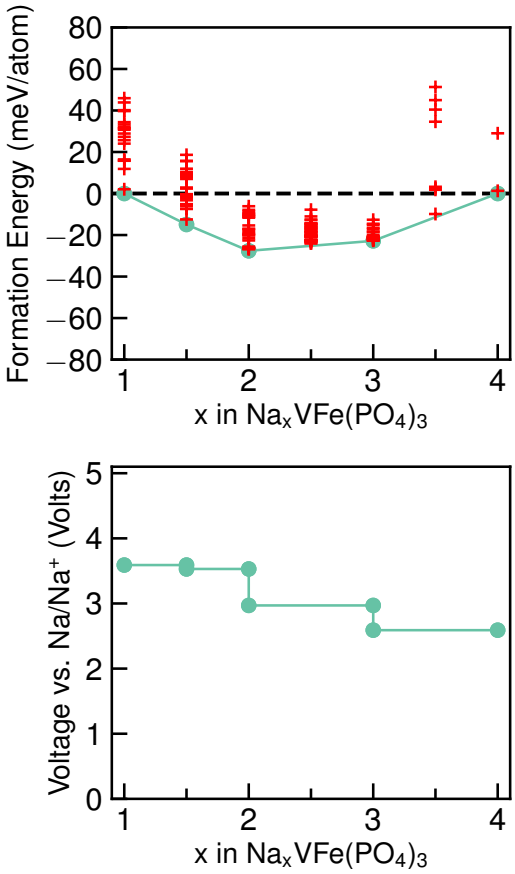

Figure S21 (upper panel) The computed formation energies and respective convex hulls (green line) for Na vacancy orderings as a function of Na concentration (x) in $Na_xVFe(PO_4)_3$. (lower panel) The corresponding intercalation voltage vs. Na/Na^+ at different Na content. Note that x varies in the range $1 \leq x \leq 4$. The stable orderings forming the convex hull are displayed as green dots while the unstable orderings are given as red symbols.

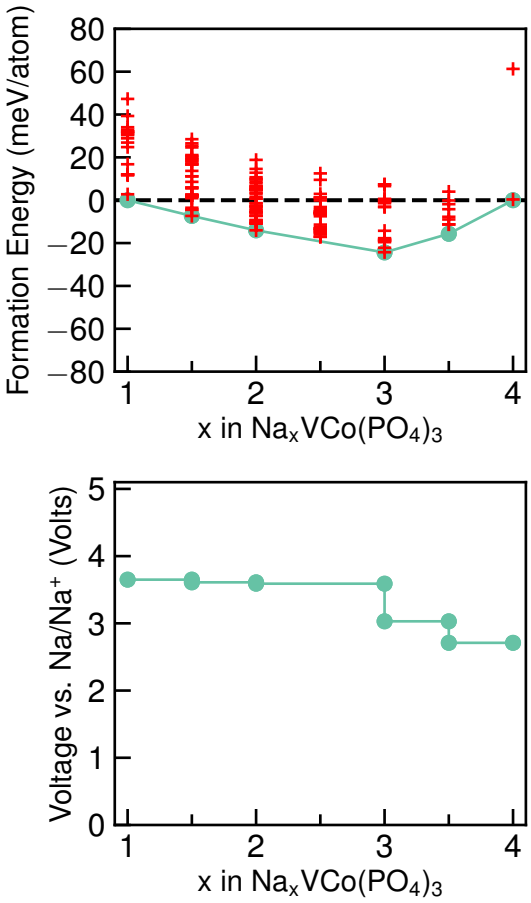

Figure S22 (upper panel) The computed formation energies and respective convex hulls (green line) for Na vacancy orderings as a function of Na concentration (x) in $Na_xVCo(PO_4)_3$. (lower panel) The corresponding intercalation voltage vs. Na/Na^+ at different Na content. Note that x varies in the range $1 \leqslant x \leqslant 4$. The stable orderings forming the convex hull are displayed as green dots while the unstable orderings are given as red symbols.

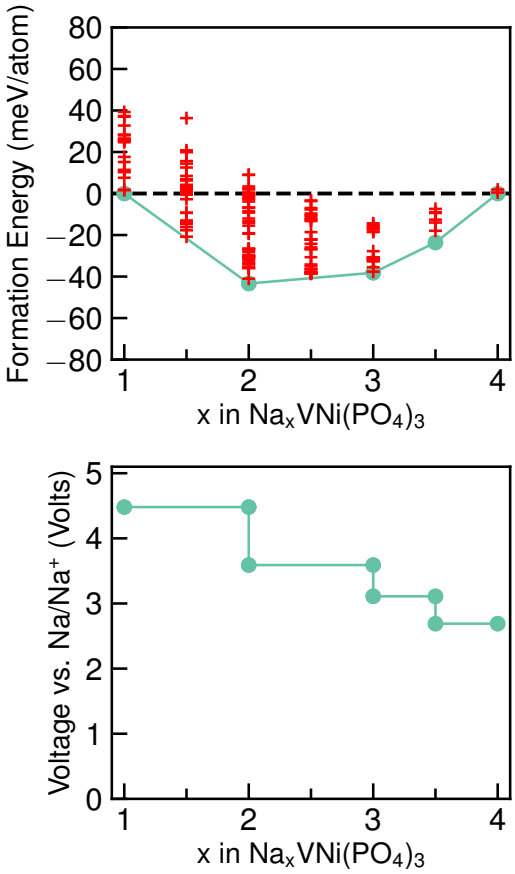

Figure S23 (upper panel) The computed formation energies and respective convex hulls (green line) for Na vacancy orderings as a function of Na concentration (x) in $Na_xVNi(PO_4)_3$. (lower panel) The corresponding intercalation voltage vs. Na/Na^+ at different Na content. Note that x varies in the range $1 \leqslant x \leqslant 4$. The stable orderings forming the convex hull are displayed as green dots while the unstable orderings are given as red symbols.

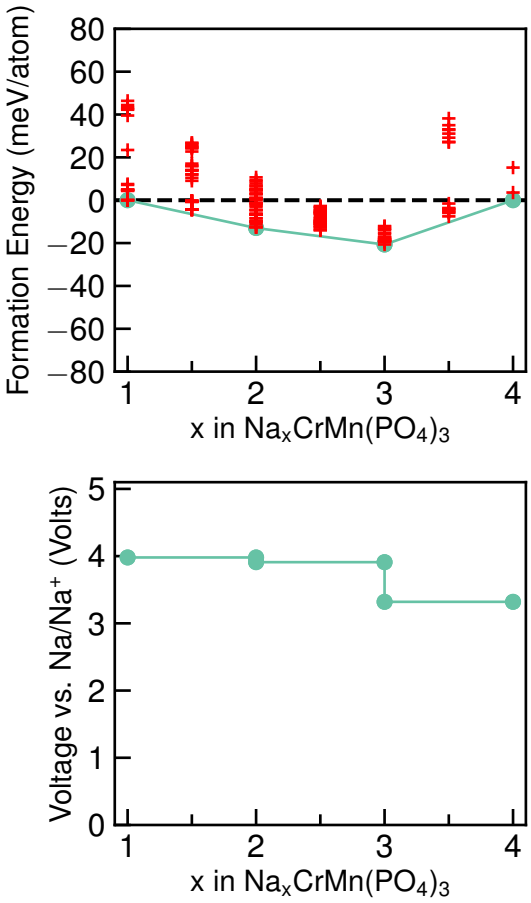

Figure S24 (upper panel) The computed formation energies and respective convex hulls (green line) for Na vacancy orderings as a function of Na concentration (x) in $Na_xCrMn(PO_4)_3$. (lower panel) The corresponding intercalation voltage vs. Na/Na^+ at different Na content. Note that x varies in the range $1 \leqslant x \leqslant 4$. The stable orderings forming the convex hull are displayed as green dots while the unstable orderings are given as red symbols.

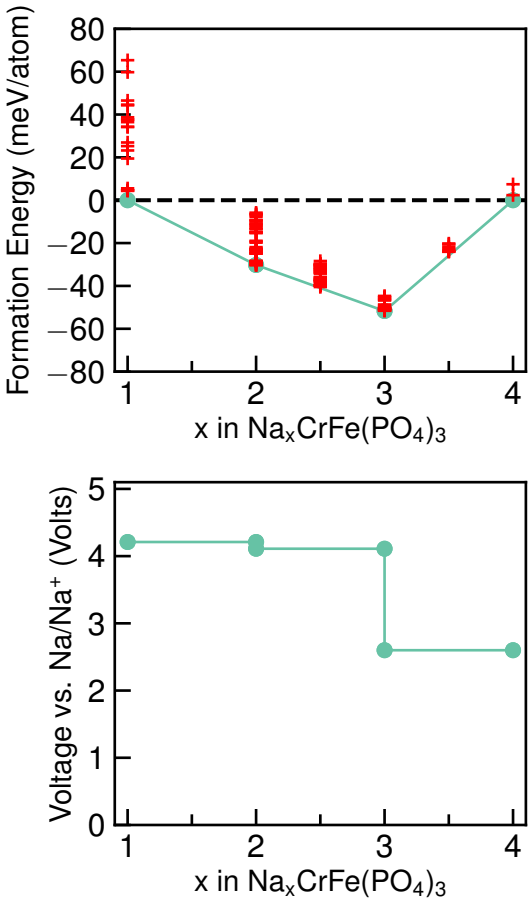

Figure S25 (upper panel) The computed formation energies and respective convex hulls (green line) for Na vacancy orderings as a function of Na concentration (x) in $Na_xCrFe(PO_4)_3$. (lower panel) The corresponding intercalation voltage vs. Na/Na^+ at different Na content. Note that x varies in the range $1 \leqslant x \leqslant 4$. The stable orderings forming the convex hull are displayed as green dots while the unstable orderings are given as red symbols.

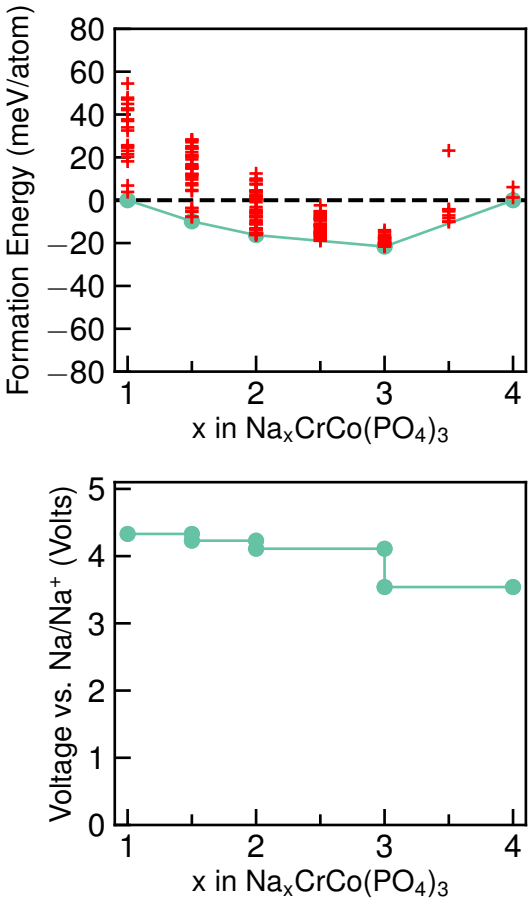

Figure S26 (upper panel) The computed formation energies and respective convex hulls (green line) for Na vacancy orderings as a function of Na concentration (x) in $Na_xCrCo(PO_4)_3$. (lower panel) The corresponding intercalation voltage vs. Na/Na^+ at different Na content. Note that x varies in the range $1 \leqslant x \leqslant 4$. The stable orderings forming the convex hull are displayed as green dots while the unstable orderings are given as red symbols.

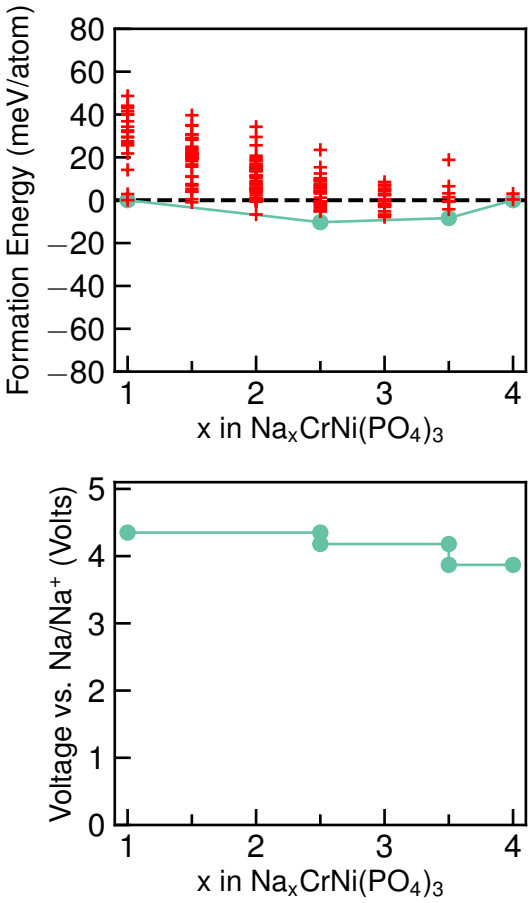

Figure S27 (upper panel) The computed formation energies and respective convex hulls (green line) for Na vacancy orderings as a function of Na concentration (x) in $Na_xCrNi(PO_4)_3$. (lower panel) The corresponding intercalation voltage vs. Na/Na^+ at different Na content. Note that x varies in the range $1 \leqslant x \leqslant 4$. The stable orderings forming the convex hull are displayed as green dots while the unstable orderings are given as red symbols.

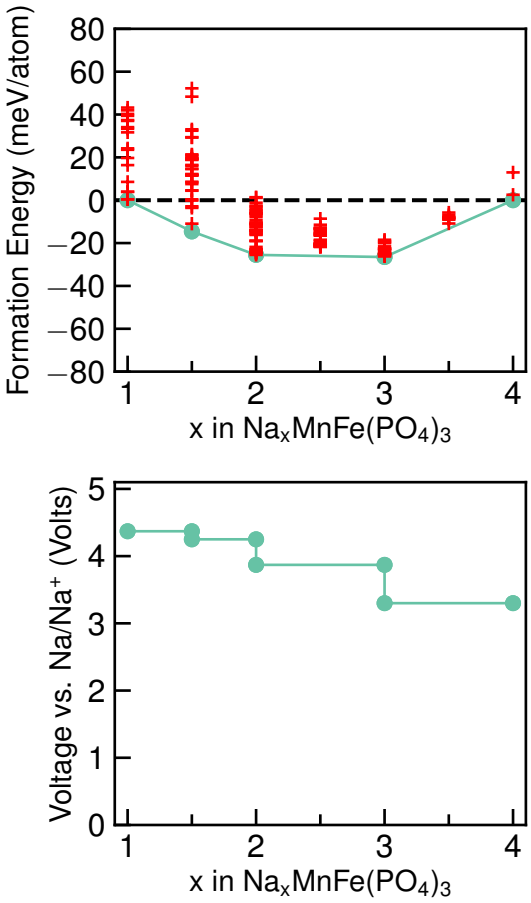

Figure S28 (upper panel) The computed formation energies and respective convex hulls (green line) for Na vacancy orderings as a function of Na concentration (x) in $Na_xMnFe(PO_4)_3$. (lower panel) The corresponding intercalation voltage vs. Na/Na^+ at different Na content. Note that x varies in the range $1 \leqslant x \leqslant 4$. The stable orderings forming the convex hull are displayed as green dots while the unstable orderings are given as red symbols.

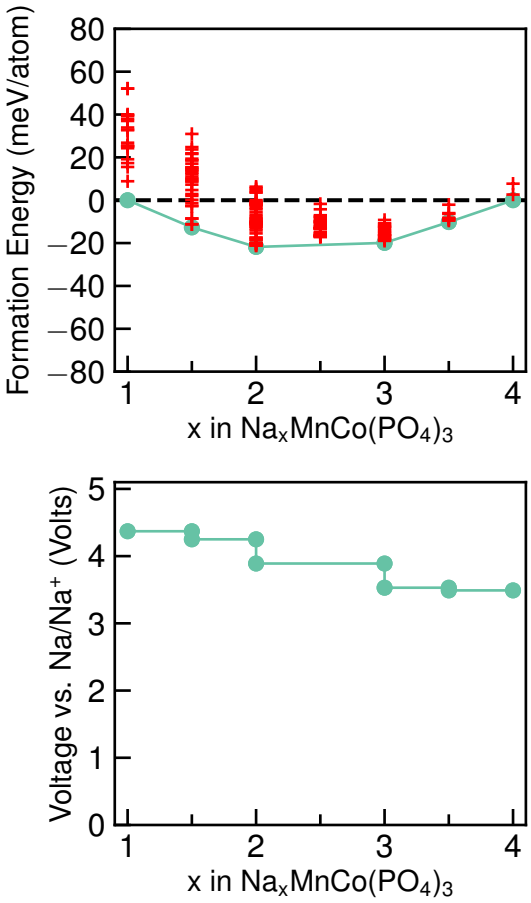

Figure S29 (upper panel) The computed formation energies and respective convex hulls (green line) for Na vacancy orderings as a function of Na concentration (x) in $Na_xMnCo(PO_4)_3$. (lower panel) The corresponding intercalation voltage vs. Na/Na^+ at different Na content. Note that x varies in the range $1 \leqslant x \leqslant 4$. The stable orderings forming the convex hull are displayed as green dots while the unstable orderings are given as red symbols.

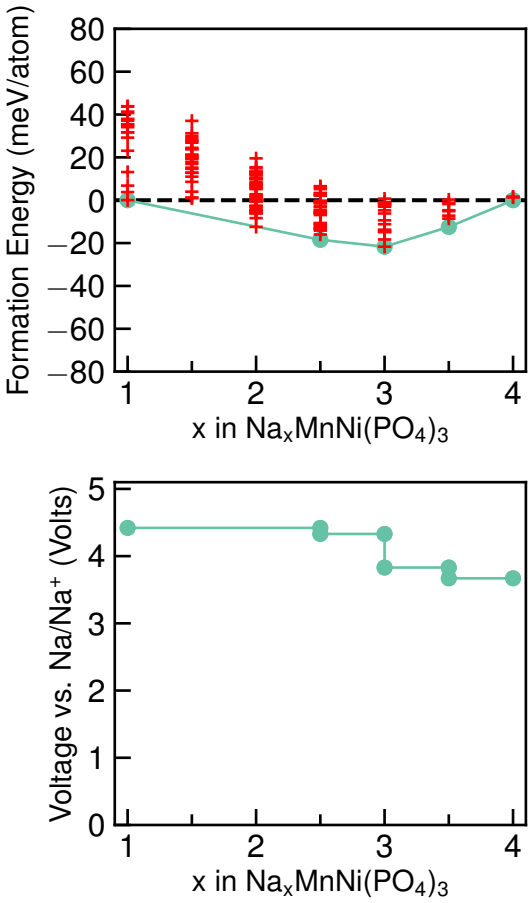

Figure S30 (upper panel) The computed formation energies and respective convex hulls (green line) for Na vacancy orderings as a function of Na concentration (x) in $Na_xMnNi(PO_4)_3$. (lower panel) The corresponding intercalation voltage vs. Na/Na^+ at different Na content. Note that x varies in the range $1 \leqslant x \leqslant 4$. The stable orderings forming the convex hull are displayed as green dots while the unstable orderings are given as red symbols.

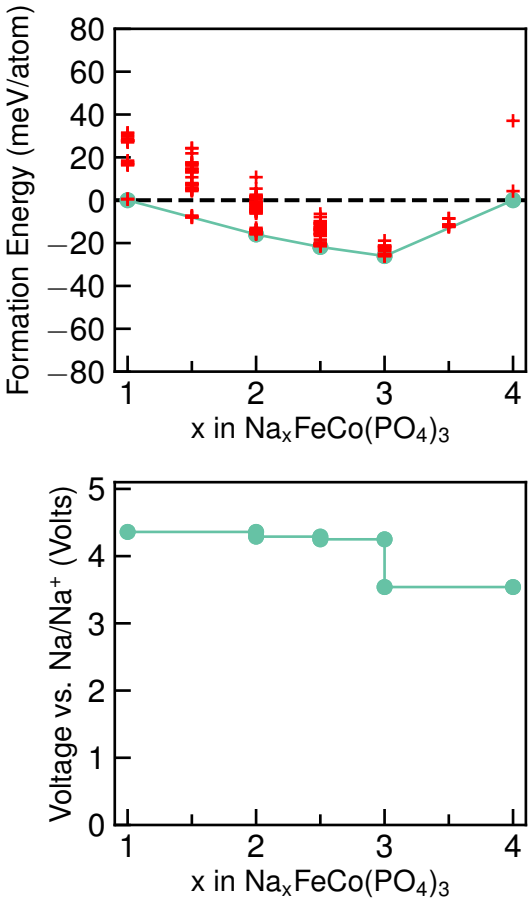

Figure S31 (upper panel) The computed formation energies and respective convex hulls (green line) for Na vacancy orderings as a function of Na concentration (x) in $Na_xFeCo(PO_4)_3$. (lower panel) The corresponding intercalation voltage vs. Na/Na^+ at different Na content. Note that x varies in the range $1 \leqslant x \leqslant 4$. The stable orderings forming the convex hull are displayed as green dots while the unstable orderings are given as red symbols.

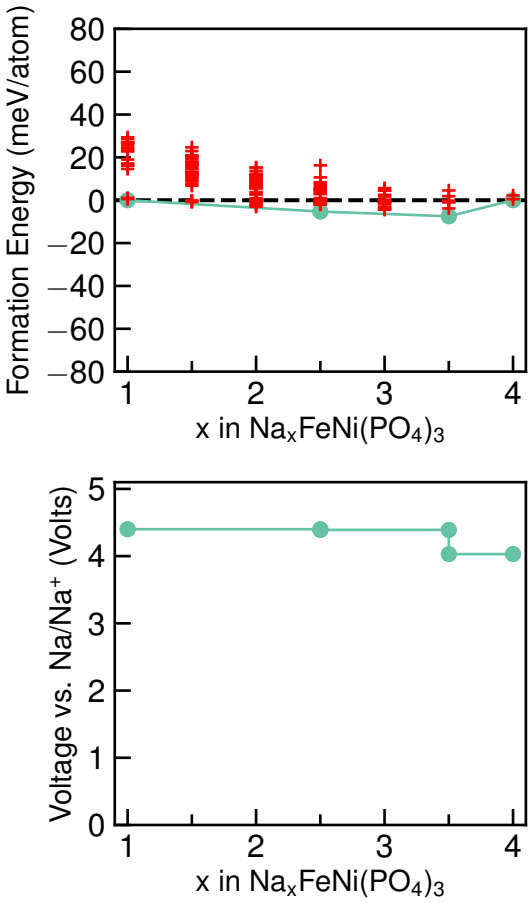

Figure S32 (upper panel) The computed formation energies and respective convex hulls (green line) for Na vacancy orderings as a function of Na concentration (x) in $Na_xFeNi(PO_4)_3$. (lower panel) The corresponding intercalation voltage vs. Na/Na^+ at different Na content. Note that x varies in the range $1 \leqslant x \leqslant 4$. The stable orderings forming the convex hull are displayed as green dots while the unstable orderings are given as red symbols.

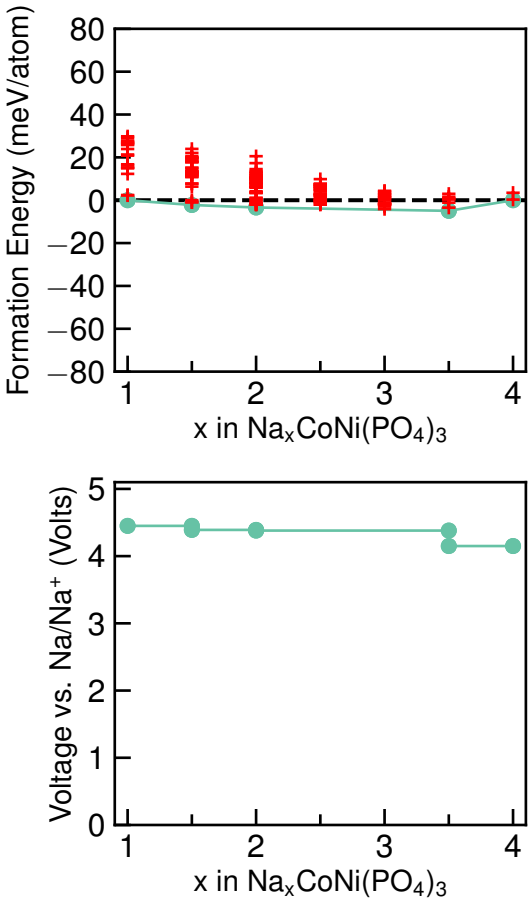

Figure S33 (upper panel) The computed formation energies and respective convex hulls (green line) for Na vacancy orderings as a function of Na concentration (x) in $Na_xCoNi(PO_4)_3$. (lower panel) The corresponding intercalation voltage vs. Na/Na^+ at different Na content. Note that x varies in the range $1 \leqslant x \leqslant 4$. The stable orderings forming the convex hull are displayed as green dots while the unstable orderings are given as red symbols.

S6 Computed Phase Diagrams of the Ni-Na-P-O system

Figure S34 shows the thermodynamics stability of various compounds in the Ni-Na-P-O phase diagram. For the sake of clarity, a reduced version of the phase diagram was plotted, also known as compound phase diagram. The red filled circles corresponds to stable phases in the global phase diagrams. The blue lines show the equilibrium among various connected compounds.

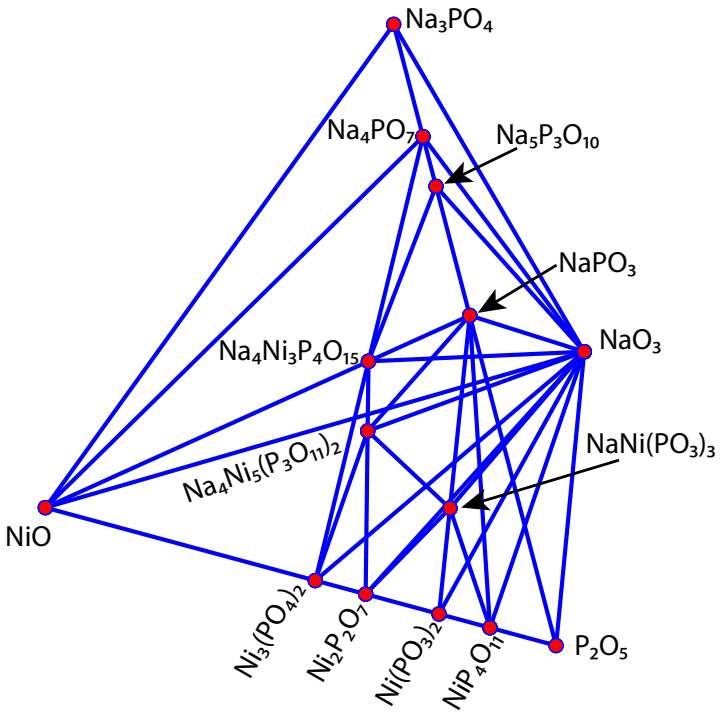

Figure S34 The computed phase diagram of chemical system Ni-Na-P-O at 0K. No stable NaSICON structures with formula $Na_xNi_2(PO_4)_3$ was observed in the global phase diagram. The compounds with compositions close to NaSICON are plotted which is in equilibrium with highly stable binaries (P_2O_5, NiO and NaO_3) and ternaries (Na_3PO_4).

In **Figure S34**, we cannot identify any stable Ni-based $Na_xNi_2(PO_4)_3$ NaSICON composition in the Ni-Na-P-O computed phase diagram.

References

1. Perdew, J. P., Burke, K. & Ernzerhof, M. Generalized gradient approximation made simple. *Phys. Rev. Lett.* **77**, 3865–3868 (1996).
2. Cococcioni, M. & De Gironcoli, S. Linear response approach to the calculation of the effective interaction parameters in the LDA+U method. *Phys. Rev. B - Condens. Matter Mater. Phys.* **71**, 035105 (2005).
3. Heyd, J., Scuseria, G. E. & Ernzerhof, M. Erratum: Hybrid functionals based on a screened Coulomb potential (Journal of Chemical Physics (2003) 118 (8207)). *Journal of Chemical Physics* **124**, 219906 (2006).
4. Lalère, F. *et al.* Improving the energy density of Na3V2(PO4)3-based positive electrodes through V/Al substitution. *J. Mater. Chem. A* **3**, 16198–16205 (2015).